Supporting Information for

Tailoring Nanostructured NiFe-LDH Catalysts via Ammonium Fluoride-Mediated Hydrothermal Synthesis: Enhanced Electrocatalytic Performance in Oxygen Evolution Reaction

Xinyi Feng[a b d], Xiaodong Hao[b] *, Xuan Zhao[c], Yangchun Guo[c], Shufang Ma[b], Bingshe Xu[b], Hui Liu[a,]*, Bo Gao[d] *

[a] *School of Materials Science and Engineering, Shaanxi University of Science & Technology, Xi'an 710021, China*

[b] *Xi'an Key Laboratory of Compound Semiconductor Materials and Devices, School of Physics & Information Science, Shaanxi University of Science & Technology, Xi' an 710021, China*

[c] *Shaanxi Key Laboratory of Chemical Additives for Industry, College of Chemistry and Chemical Engineering, Shaanxi University of Science & Technology, Xi'an 710021, China*

[d] *Institute of Orthopaedic Surgery, Xijing Hospital, Air Force Military Medical University, Xi'an 710032, China.*

*Corresponding author:

hao.xiaodong@sust.edu.cn；liuhui@sust.edu.cn；gaobofmmu@hotmail.com

1. Experimental Section

1.1 Chemical and Materials.

Nickel nitrate hexahydrate ($Ni(NO_3)_2·6H_2O$), iron nitrate nonahydrate ($Fe(NO_3)_3·9H_2O$), urea (CH_4N_2O), ammonium fluoride (NH_4F), potassium hydroxide (KOH), and a 5% Nafion solution were all purchased from Aladdin Chemical Reagent Company. Deionized water was collected via a purification system. All reagents were used as received without further purification.

1.2 Preparation of NiFe-LDH via a one-step hydrothermal method.

A 0.2 M solution of $Ni(NO_3)_2·6H_2O$, a 0.05 M solution of $Fe(NO_3)_3·9H_2O$, and a 1.25 M solution of urea were each mixed thoroughly in 10 ml, followed by the addition of different volumes of 2.5 M NH_4F solution and the appropriate amount of deionized water to achieve a total solution volume of 40 ml. The well-mixed solution was transferred to a stainless-steel autoclave lined with polytetrafluoroethylene and subjected to hydrothermal treatment at 120 °C for 12 hours. After cooling to room temperature, the resulting material was washed several times with deionized water and anhydrous ethanol, followed by overnight drying at 60°C to obtain the composite material. The obtained samples were named NFL-*x*F (where *x* represents the amount of NH_4F added, corresponding to 0, 1, 3, 5, 7, and 9 times the concentration of Fe^{3+} ions). Under the same conditions, *β*-$Ni(OH)_2$ and *β*-FeOOH were prepared as the control samples by omitting either the Fe precursor or the Ni precursor.

1.3 Materials characterizations.

The crystalline structure of the as-synthesized samples was investigated using X-ray diffraction (XRD) with a Bruker D8 X-ray diffractometer equipped with a Cu target Kα radiation source. The morphology of the samples was observed using scanning electron microscopy (SEM) with a Hitachi S-800 instrument. The microstructure and crystal structure of the samples were examined using transmission electron microscopy (TEM) with a JEOL-JEM 2100 Plus instrument, and high-resolution TEM characterization was conducted using a double spherical aberration-corrected transmission electron microscope (JEOL-ARM 300F) in TEM mode. X-ray photoelectron spectroscopy (XPS) was employed to study the binding energies of Ni 2p, Fe 2p, and O 1s in different samples, with binding energy calibrated using C 1s (284.8 eV) and elemental valence state changes simulated using Avantage software. Fourier-transform infrared spectroscopy (FT-IR) characterization was performed as well.

1.4 Electrochemical tests.

The electrochemical performance of the samples was tested using a standard three-electrode system on an electrochemical workstation (Shanghai Chenhua, CHI660E). The three electrodes consisted of a working electrode (glassy carbon electrode loaded with active material, diameter 0.3 cm), a reference electrode (Ag/AgCl in 3 M KCl solution), and a counter electrode (platinum wire). The electrolyte used during testing was a 1 M KOH solution, and prior to testing, high-purity nitrogen gas was continuously bubbled into the electrolyte for 30 minutes to remove oxygen. The electrode activation process was conducted using cyclic voltammetry (CV) with a scan range of −0.1 V to 0.9 V at a scan rate of 5 mV·s⁻¹until the electrode reached a steady

state. Subsequently, linear sweep voltammetry (LSV) was performed at a scan rate of 1 mV·s^{-1}. Electrochemical impedance spectroscopy was conducted over a frequency range from 100 kHz to 0.1 Hz, and 85% iR compensation was applied to all polarization curves to correct for solution resistance. Furthermore, all potentials were converted to the reversible hydrogen electrode (RHE) scale using the Nernst equation:

$$E_{RHE} = E_{Ag/AgCl} + 0.0592 \times pH + E_{0Ag/AgCl}$$

where E_{RHE} represents the potential relative to RHE, $E_{Ag/AgCl}$ is the experimental potential measured relative to Ag/AgCl, $E_{0Ag/AgCl}$ is the standard potential of the Ag/AgCl reference electrode at room temperature (25 ± 1 °C), measured as 0.195 V in this work. The stability of the electrodes was evaluated through chronoamperometry at a current density of 120 mA·cm^{-2}.
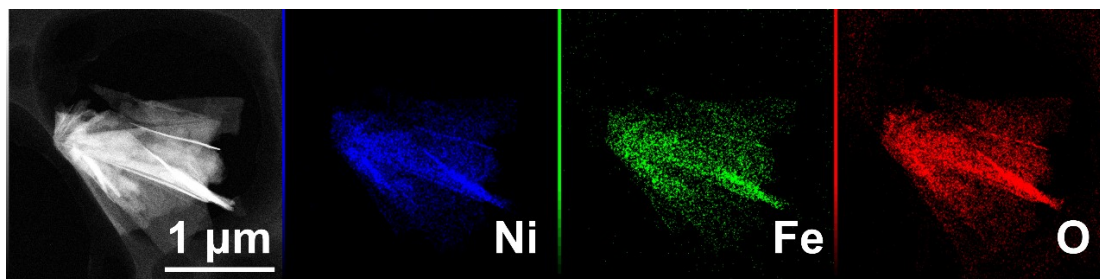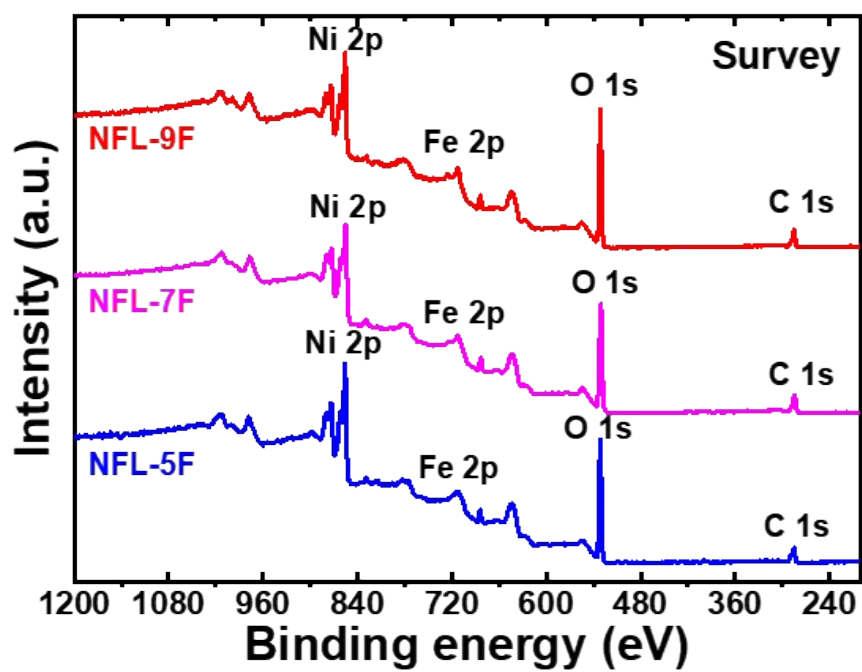
Supplementary Figures
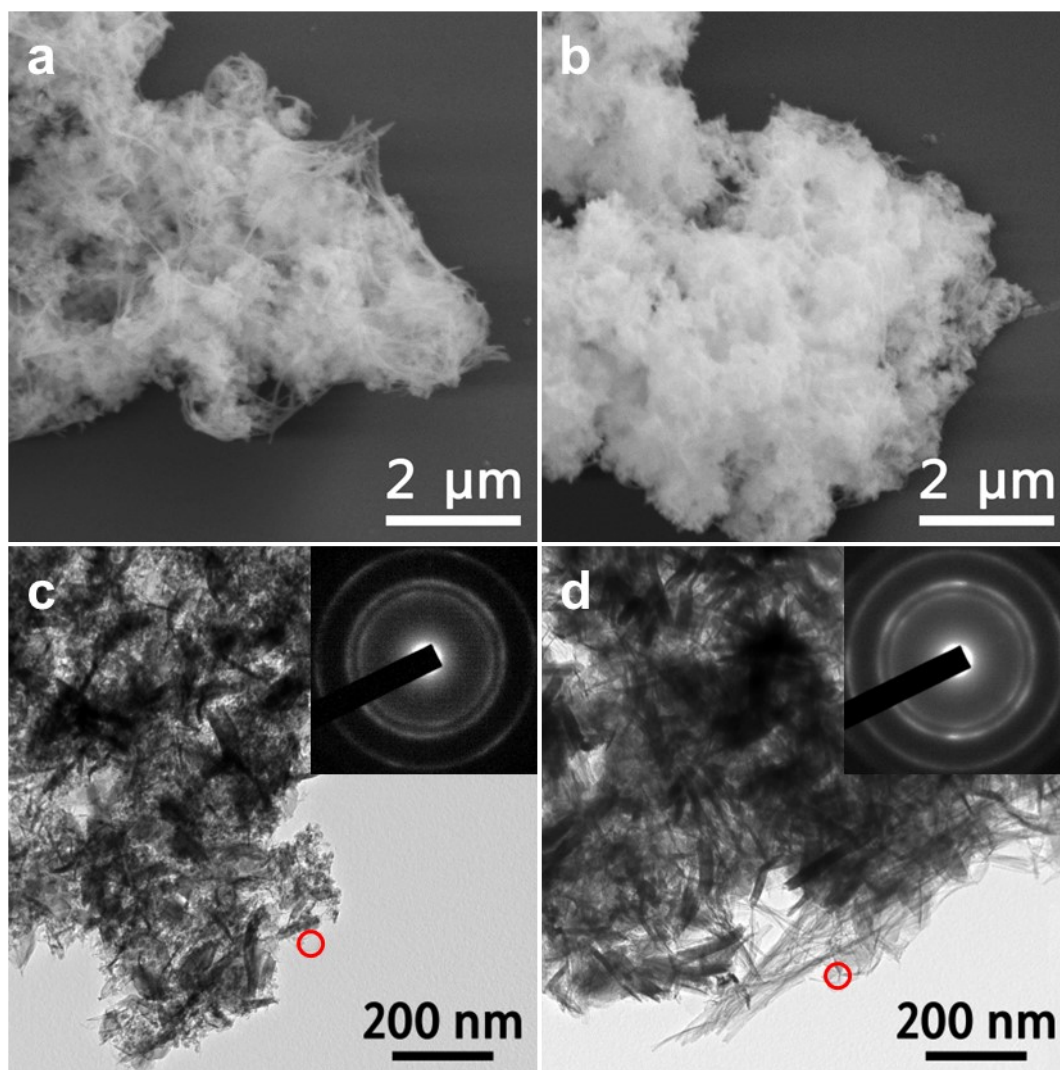
Figure S1. SEM image, TEM image and insert the FFT pattern of (a, c) NFL-0F, (b, d) NFL-1F.
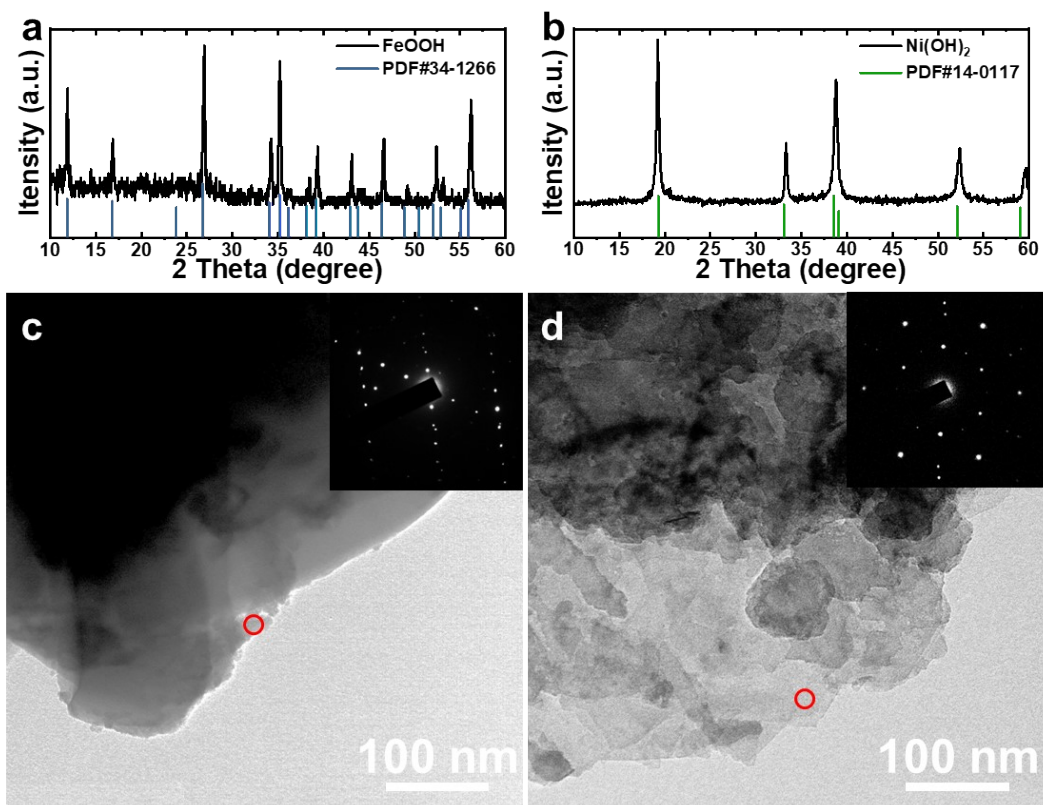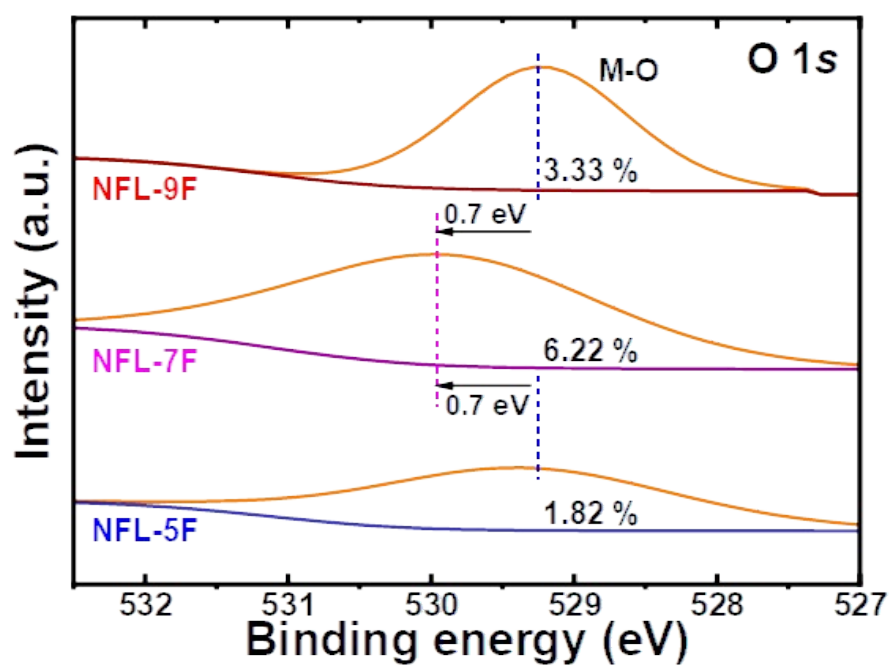
Figure S2. XRD patterns of (a) β-Ni(OH)$_2$ and (b) β-FeOOH; TEM image and insert the FFT pattern of (c) β-Ni(OH)$_2$, (d) β-FeOOH.
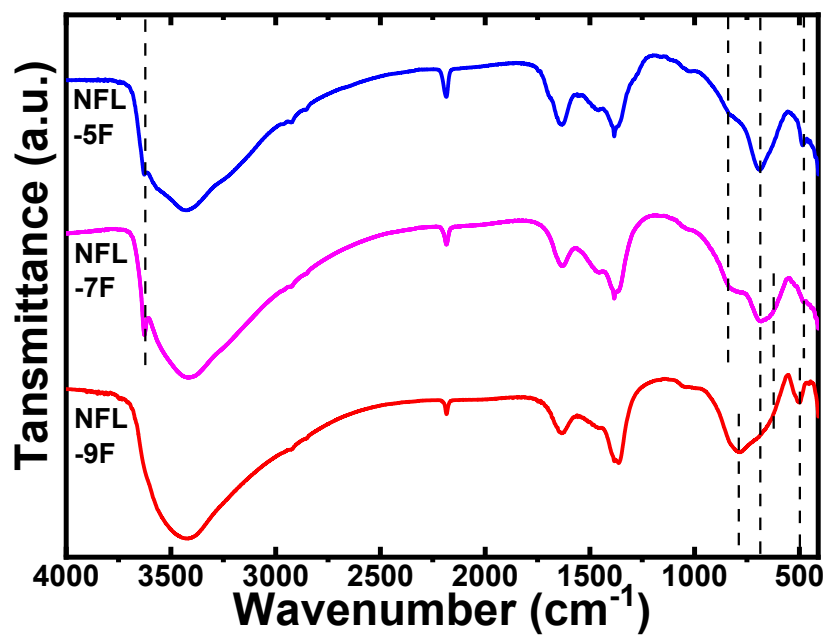
Figure S3. The EDS elemental mapping of the Ni *K*-edge, Fe *L*-edge and O *K*-edge of NFL-7F.
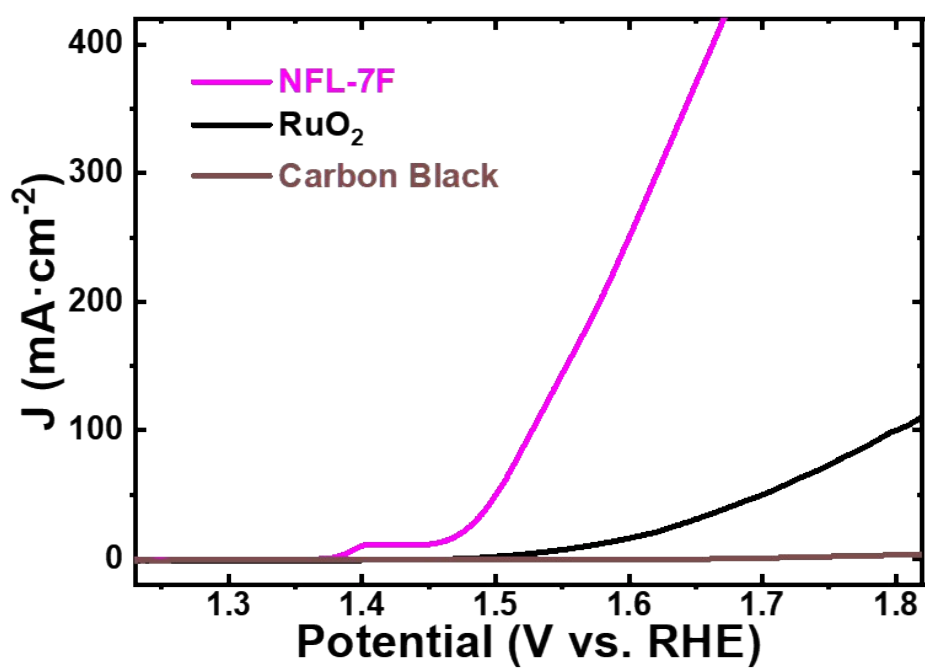
Figure S4. The XPS survey spectra of NFL-5F, NFL-7F and NFL-9F.

Figure S5. Comparison of M-O bonds of O1s in XPS spectra of NFL-5F, NFL-7F and NFL-9F.

Figure S6. FT-IR spectra of NFL-5F, NFL-7F and NFL-9F.

Figure S7. LSVs of NFL-7F, RuO_2 and Carbon Black for catalyzing OER in 1.0 M KOH
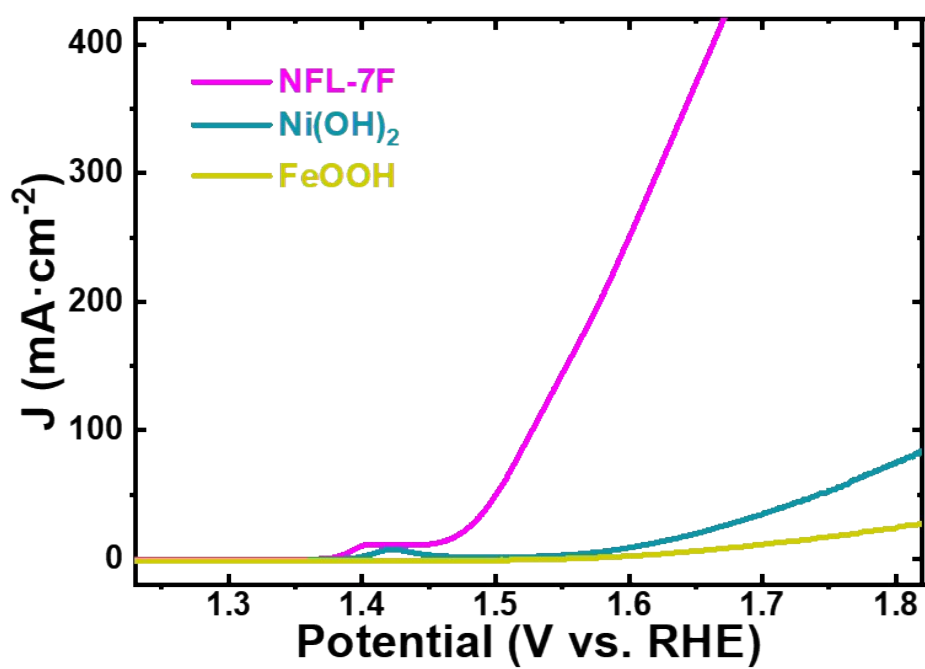
Figure S8. LSVs of NFL-7F, β-Ni(OH)$_2$ and β-FeOOH for catalyzing OER in 1.0 M KOH
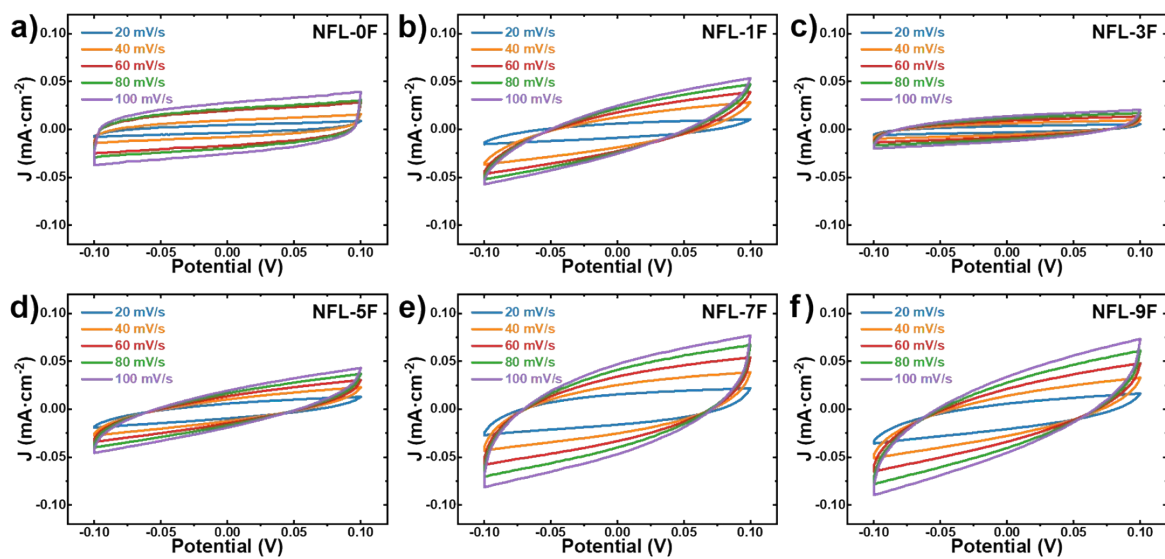
Figure S9. CV curves at different scan rates for (a) NFL-0F, (b) NFL-1F, (c) NFL-3F, (d) NFL-5F, (e) NFL-7F, and (f) NFL-9F.

Figure S10. Comparison of XRD characterization profiles before and after it test.

Figure S12. TEM image of NFL-7F after it test.

Table S1. Comparison with reported state-of-the-art catalysts for the oxygen evolution reaction.

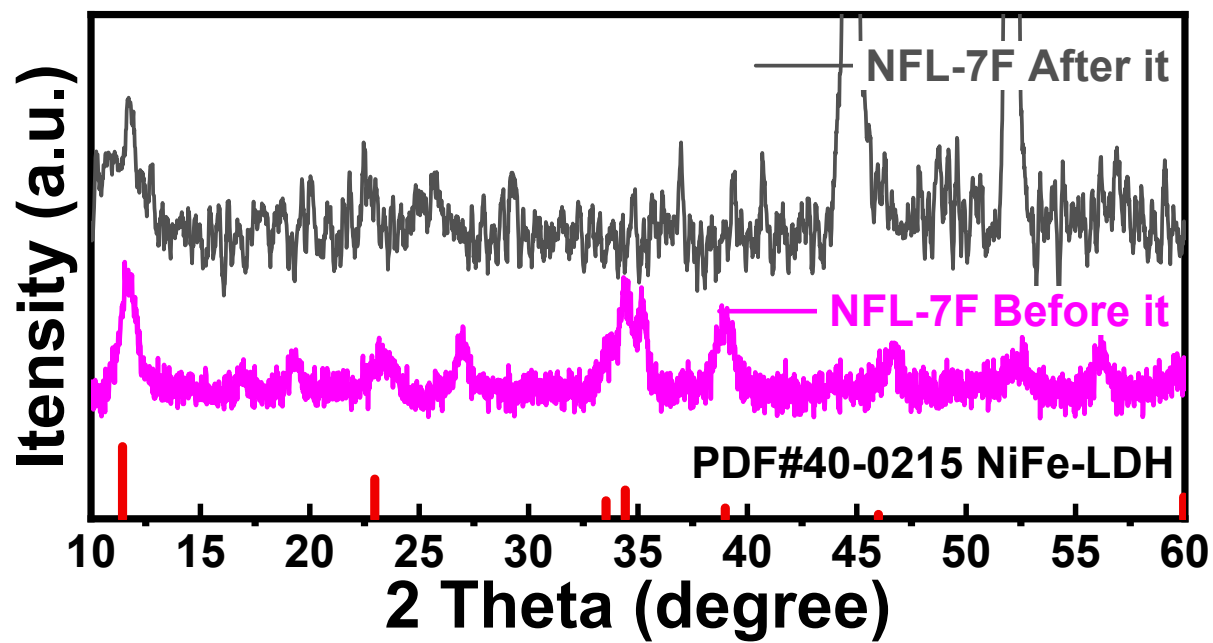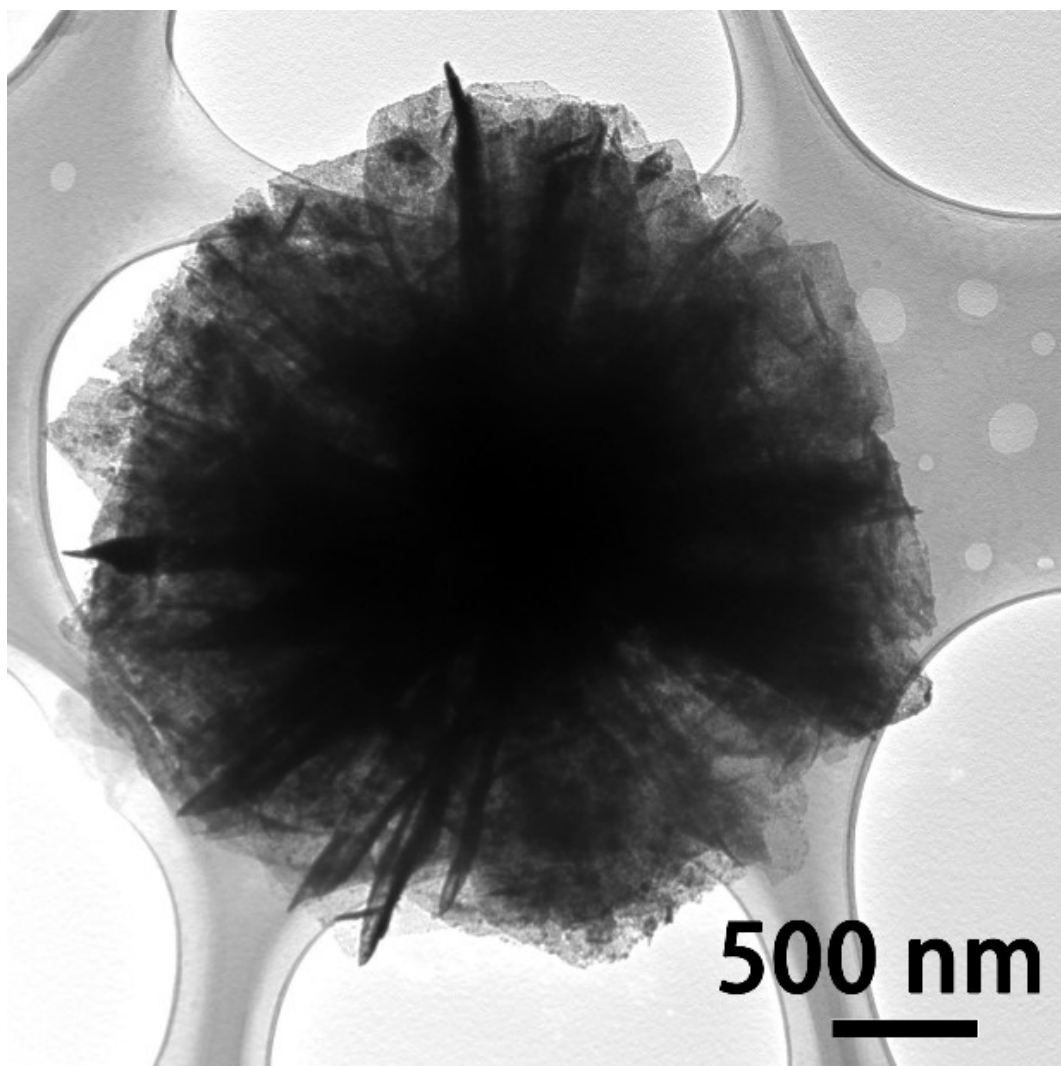| Catalyst	Overpotential at 50 mA·cm^{-2} (mV)	Tafel slope (mV·dec^{-1})	References
Ni^{vac}Fe^{vac}-LDH	310	52	[1]
NiFe-25°	330	48.7	[2]
NiFe$_{III}$(1:1)	382	31.1	[3]
NiFe-LDH pyramid electrode	310	66	[4]
r-NiFe LDH	320	83	[5]
PR-NiFe LDH	330	75	[6]
NiFe25/PGS	362	33	[7]
10-NiFe LDH/CNTs	280	30	[8]
NiFe LDH-Ni(III)Li	280	35	[9]
Ni-BDC@NiFe-LDH-2	310	45	[10]
Ni$_2$Fe$_1$-LDH/rGO/NF	300	37.9	[11]
MIL-101@NiFe-LDH	340	61.1	[12]
NiFe-LDH-Ti$_4$O$_7$	350	35	[13]
Ni/LDH-ZnO (2 min)	310	57	[14]
NFO/3DGN-10	355	64	[15]
NFL-7F	**270**	**68.1**	**This work**

References

(1) Peng, L.; Yang, N.; Yang, Y.; Wang, Q.; Xie, X.; Sun-Waterhouse, D.; Shang, L.; Zhang, T.; Waterhouse, G. I. N., Atomic Cation-Vacancy Engineering of NiFe-Layered Double Hydroxides for Improved Activity and Stability towards the Oxygen Evolution Reaction. *Angew. Chem. Int. Ed.* **2021,** *60* (46), 24612-24619.

(2) Rinawati, M.; Wang, Y.-X.; Chen, K.-Y.; Yeh, M.-H., Designing a spontaneously deriving NiFe-LDH from bimetallic MOF-74 as an electrocatalyst for oxygen evolution reaction in alkaline solution. *Chem. Eng. J.* **2021,** *423*, 130204.

(3) Huang, F.; Yao, B.; Huang, Y.; Dong, Z., NiFe layered double hydroxide nanosheet arrays for efficient oxygen evolution reaction in alkaline media. *Int. J. Hydrogen Energy* **2022,** *47* (51), 21725-21735.

(4) Ahn, J.; Park, Y. S.; Lee, S.; Yang, J.; Pyo, J.; Lee, J.; Kim, G. H.; Choi, S. M.; Seol, S. K., 3D-printed NiFe-layered double hydroxide pyramid electrodes for enhanced electrocatalytic oxygen evolution reaction. *Scientific Reports* **2022,** *12* (1), 346.

(5) Hou, X.; Li, J.; Zheng, J.; Li, L.; Chu, W., Introducing oxygen vacancies to NiFe LDH through electrochemical reduction to promote the oxygen evolution reaction. *Dalton Trans.* **2022,** *51* (36), 13970-13977.

(6) Wen, Q.; Wang, S.; Wang, R.; Huang, D.; Fang, J.; Liu, Y.; Zhai, T., Nanopore-rich NiFe LDH targets the formation of the high-valent nickel for enhanced oxygen evolution reaction. *Nano Res.* **2023,** *16* (2), 2286-2293.

(7) Gozzo, C. B.; Soares, M. R. S.; Destro, F. B.; Junior, J. B. S.; Leite, E. R., Facile deposition of NiFe-LDH ultrathin film on pyrolytic graphite sheet for oxygen evolution reaction in alkaline electrolyte. *Int. J. Hydrogen Energy* **2022,** *47* (14), 8786-8798.

(8) Duan, M.; Qiu, M.; Sun, S.; Guo, X.; Liu, Y.; Zheng, X.; Cao, F.; Kong, Q.; Zhang, J., Intercalating assembly of NiFe LDH nanosheets/CNTs composite as high-performance electrocatalyst for oxygen evolution reaction. *Appl. Clay Sci.* **2022,** *216*, 106360.

(9) Xu, Z.; Ying, Y.; Zhang, G.; Li, K.; Liu, Y.; Fu, N.; Guo, X.; Yu, F.; Huang, H., Engineering NiFe layered double hydroxide by valence control and intermediate stabilization toward the oxygen evolution reaction. *J. Mater. Chem. A* **2020,** *8* (48), 26130-26138.

(10) Dong, Q.; Shuai, C.; Mo, Z.; Guo, R.; Liu, N.; Liu, G.; Wang, J.; Liu, W.; Chen, Y.; Liu, J.; Jiang, Y.; Gao, Q., The in situ derivation of a NiFe-LDH ultra-thin layer on Ni-BDC nanosheets as a boosted electrocatalyst for the oxygen evolution reaction. *CrystEngComm* **2021,** *23* (5), 1172-1180.

(11) Wang, K.; Guo, J.; Zhang, H., Synergistic effect of nanosheet-array-like NiFe-LDH and reduced graphene oxide modified Ni foam for greatly enhanced oxygen evolution reaction and hydrogen evolution reaction. *Mater. Adv.* **2022,** *3* (17), 6887-6896.

(12) Huang, J.; Li, K.; Wang, L.; She, H.; Wang, Q., In situ conversion builds MIL-101@NiFe-LDH heterojunction structures to enhance the oxygen evolution reaction. *Chin. Chem. Lett.* **2022,** *33* (8), 3787-3791.

(13) Ibrahim, K. B.; Su, W. N.; Tsai, M. C.; Kahsay, A. W.; Chala, S. A.; Birhanu, M. K.; Lee, J. F.; Hwang, B. J., Heterostructured composite of NiFe-LDH nanosheets with Ti4O7 for oxygen evolution reaction. *Mater. Today Chem.* **2022,** *24*, 100824.

(14) Luo, Y.; Wu, Y.; Wu, D.; Huang, C.; Xiao, D.; Chen, H.; Zheng, S.; Chu, P. K., NiFe-Layered Double Hydroxide Synchronously Activated by Heterojunctions and Vacancies for the Oxygen Evolution Reaction. *ACS Appl. Mater. Interfaces* **2020,** *12* (38), 42850-42858.

(15) Zhang, P.; Chen, L.; Ge, L.; Song, P.; Xie, R.; Wang, B.; Fu, Y.; Jia, S.; Liao, T.; Xiong, Y., A 3D rGO-supported $NiFe_2O_4$ heterostructure from sacrificial polymer-assisted exfoliation of NiFe-LDH for efficient oxygen evolution reaction. *Carbon* **2022,** *200,* 422-429.